Large scale air–sea interactions with a simple general circulation model

By RICK SALMON and MYRL C. HENDERSHOTT, *Scripps Institution of Oceanography, La Jolla, California, USA*

(Manuscript received January 2; in final form March 11, 1975)

ABSTRACT

We have coupled Lorenz's (1960) two-layer atmospheric model to a "copper plate" ocean to obtain a simple model that can be used to study the effects of large-scale sea surface temperature (SST) anomalies on the dynamics of the atmosphere. With 164 degrees of freedom, the atmospheric model mimics the observed northern hemisphere energy cycle in fair detail. In three experiments, each lasting one year, we consider an ocean (*a*) with fixed temperature that depends only on latitude; (*b*) with fixed large-amplitude SST anomalies; and (*c*) with temperature determined by heat exchange with the air. Only in (*b*) are significant dynamical effects observed. These consist of a weak monsoon response in the subtropics and a tendency for storms to intensify over warm water at higher latitude. Experiment (*c*) developed SST anomalies that resemble the observed anomalies; however, the atmosphere and ocean in (*c*) differ insignificantly from the atmosphere and re-computed "slave ocean" in (*a*), even when the flows are averaged in reference frames moving with the anomalies. Our results suggest that the atmosphere may be too noisy to be much affected by SST anomalies on time scales over which the anomalies are themselves predictable.

1. Introduction

We wish to study the effects of large-scale sea surface temperature anomalies, such as those described by Namias (1959), on the dynamics of the overlying atmosphere. By "anomaly" we mean the instantaneous departure of the sea surface temperature (SST) from its long-term time average. The persistence of SST anomaly patterns over time scales of months has led many people to believe that a better knowledge of these anomalies and their influence on the atmosphere could lead to improvements in long-term weather predictions. However, the associated heating anomalies are very small compared to many of the other fluxes that balance the heat budget of an atmospheric column; and it has therefore proved difficult to envision specific mechanisms by which SST anomalies might affect the weather. Our task is to weigh the relative importance of these two opposing features: long term persistence versus weakness of the signal.

The problem is complicated by the atmosphere's intrinsic lack of exact predictability. By this we mean that the equations governing atmospheric motion are ill-posed with respect to initial value problems in the sense that perturbations in the initial conditions at the smallest scales lead to completely different solutions after finite times. The cause of the growing difference is the propagation of the initial perturbation from the smallest to the largest scales of motion via the nonlinear terms in the Navier-Stokes equations. We can define an atmospheric predictability time scale, T_A, as the time required for a perturbation in the flow at the scale of the separation between weather observing stations to reach the largest scales of motion. Theoretical and numerical estimates for T_A range between 5 days and about 3 weeks.

The existence of a limiting predictability time, T_A, for the atmosphere has important implications for the problem under study. First, it underscores the importance of studying forcing fields (such as SST) which have themselves a predictability time that is longer than T_A. The predictability time for sea surface temperature, T_0, is of the order of months because of the high heat capacity of the oceanic mixed

layer and its relatively sluggish motion. Thus,

$$T_0 > T_A$$

and knowledge of the SST pattern ought to permit forecasts longer than T_A *provided* there is some *significant* connection between SST state and the state of the atmosphere above.

However, the limit on exact predictability suggests that this connection might at best be statistical. Consider the following hypothetical experiment: Imagine an ideal atmosphere whose external forcing fields (continents, oceans, solar heating, etc.) are freely controlled by us. Let $V(t)$ be any functional of the state of the atmosphere at time t. Let (1) denote some standard state for the forcing fields and let (2) denote some other forcing state (for example, a state with fixed SST anomalies). Now imagine two experiments beginning from the same initial conditions but subject to the different forcing conditions (1) and (2). Let $V_1(t)$ and $V_2(t)$ be the outcomes of these experiments.

We should not be surprised if, after times longer than T_A, the two outcomes no longer resemble one another. However, it is misleading to attribute all of the difference $V_1 - V_2$ to the different forcing conditions (1) and (2). At any time, in fact, the major part of $V_1 - V_2$ is apt to be random, i.e. unpredictable; but we are interested only in that part of $V_1 - V_2$ that can be predicted. The predictable part of $V_1 - V_2$ will not be removed by statistical averaging. Therefore, we should compare not the outcomes themselves but rather their statistics.

It is plausible that the statistics of V depend only on the forcing (not on the initial conditions) and that the statistics change when the forcing changes. However, we should still want to know whether the statistical difference between V_1 and V_2 is large or small compared to the likely random differences.

For fixed forcing conditions, $V(t)$ is a stationary stochastic process with ensemble mean $\langle V \rangle$ which is independent of time. We find $\langle V \rangle$ by averaging $V(t)$ over many realizations, or, as is commonly done, by assuming $V(t)$ to be ergodic and averaging in time. The time-average estimator

$$\bar{V}_T = \frac{1}{T}\int_0^T V(t)\,dt$$

is a random variable with expected value $\langle V \rangle$ and standard deviation proportional to $T^{-\frac{1}{2}}$ for large enough T.[1] That is, the average of V over a record of length T is "within" const/$T^{\frac{1}{2}}$ of $\langle V \rangle$.

Now suppose $\langle V_1 \rangle$ and $\langle V_2 \rangle$ are the ensemble averages of V subject to the different fixed forcing conditions. Then the time, T_s, required for a change in forcing from state (1) to state (2) to make itself felt above the natural noisiness in V is given roughly by:

$$|\langle V_1 \rangle - \langle V_2 \rangle| = \text{const}_1/T_s^{1/2} + \text{const}_2/T_s^{1/2}$$

We might call T_s the "significance time scale" for V.

The pertinence of T_s to our problem is that if $T_s > T_0$ for any realizable change in SST state, then such changes are useless as long term predictors of V because they are themselves destroyed by random processes before they can produce statistically significant changes in V. If, on the other hand, $T_0 > T_s$, then the field of SST may be a useful predictor of the quantity V. Said another way: if $T_0 > T_s$, then the long persistence of SST anomalies overcomes the weakness of their heat fluxes; but if $T_s > T_0$, then the opposite is true.

By means of a mathematical model, we can, in principle, estimate the quantities $\langle V \rangle$, const, and T_s and thereby determine if and how knowledge of SST anomalies can help to extend forecasts. In the following pages we present the tentative results of such a study. By way of overall summary, we find that, for several quantities of interest studied in our simple model, T_s is of the order of T_0 or longer, so that knowledge about SST anomalies would not greatly extend forecasts. However, our conclusions depend on the many simplifying assumptions we have made and may well be altered by future work.

2. The model

We are interested in the behavior of the coupled ocean/atmosphere system over time scales of months—the time scales in which SST anomalies are observed to appear and dis-

[1] T is large enough if $\tau > T \Rightarrow |R(\tau)| \ll 1$ where $R(\tau) = \dfrac{\langle V(t)\,V(t+\tau)\rangle - \langle V\rangle^2}{\langle V^2\rangle - \langle V\rangle^2}$ is the autocorrelation of V. See section 3 for a further discussion.

appear. Such times are long compared to T_A and to the energy transit time through the atmospheric spectrum. Consequently, we require a somewhat sophisticated model for the atmosphere—one that correctly simulates the many nonlinear processes that maintain the global general circulation against dissipation. In order to accommodate nonlinear transfers of energy over a range of scales, the atmospheric model must be a numerical one. As such, it must be both economical and computationally stable with respect to the relatively long time integrations required for statistical averaging. To satisfy these requirements, we have adopted a simple atmospheric model invented by Lorenz (1960).

Our ocean model can likely be far simpler, because a time scale of months is possibly still short compared to the time required for ocean currents to greatly alter an SST anomaly pattern whose features are several thousand kilometers in diameter. To begin with, we will ignore ocean motion altogether; our model ocean will be a stationary heat reservoir covering the globe.

In the two-layer version of Lorenz's atmospheric model the dependent variables are:

$\psi + \tau$ the stream function at 250 mb,

$\psi - \tau$ the stream function at 750 mb,

$\theta + \sigma$ the potential temperature at 250 mb,

$\theta - \sigma$ the potential temperature at 750 mb,

$\chi \equiv -\frac{1}{\Delta p}\int_0^{\Delta p} \phi(p)\,dp$ the vertical average of the velocity potential ϕ (Δp = 500 mb).

In terms of the above variables, the two-layer equations take the form:

$$\nabla^2\psi_t + J(\psi, \nabla^2\psi + f) + J(\tau, \nabla^2\tau) = F_\psi \tag{1}$$

$$\nabla^2\tau_t + J(\tau, \nabla^2\psi + f) + J(\psi, \nabla^2\tau) - \nabla\cdot(f\nabla\chi) = F_\tau \tag{2}$$

$$\theta_t + J(\psi, \theta) + J(\tau, \sigma) - \nabla\cdot(\sigma\nabla\chi) = H_\theta \tag{3}$$

$$\sigma_t + J(\psi, \sigma) + J(\tau, \theta) - \nabla\theta\cdot\nabla\chi = H_\sigma \tag{4}$$

$$bC_p\nabla^2\theta = \nabla\cdot(f\nabla\tau) \tag{5}$$

where

$$b = \tfrac{1}{2}\{(\tfrac{3}{4})^\varkappa - (\tfrac{1}{4})^\varkappa\} = 0.124$$

and

$$\varkappa \equiv R/C_p \equiv \text{(gas constant)/(heat capacity at constant pressure)}.$$

Here F_ψ, F_τ, H_θ, H_σ are the friction and heating terms. The above equations are very nearly the conventional quasi-geostrophic approximation, except that the variability of coriolis parameter, f, is retained in all terms. The method of vertical differencing incorporates the boundary conditions $\omega \equiv dp/dt = 0$ at p = 1 000 mb and $p = 0$. The vertical velocity at 500 mb is assumed to be $\omega_{500} = \Delta p\nabla^2\chi$.

Lorenz showed that, under adiabatic conditions, the eqs. (1–5) conserve the sum of

$$K = \frac{\Delta p}{g}[\nabla\psi\cdot\nabla\psi + \nabla\tau\cdot\nabla\tau] \tag{6}$$

and

$$A = \frac{2bC_p\Delta p}{g}\,\frac{[(\theta')^2 + (\sigma')^2]}{[\sigma] + [\sigma + (\theta')^2 + (\sigma')^2]^{1/2}} \tag{7}$$

which are the vertical-finite-difference analogs of the kinetic and available potential energy per unit area. Here, the brackets ([ ]) denote the area average over a region on whose boundary the normal velocity vanishes; and

$$\theta' \equiv \theta - [\theta],\ \sigma' \equiv \sigma - [\sigma]$$

The requirement that the vertically-differenced eqs. (1–5) conserve quantities that are analogous to the adiabatic invariants of the exact equations accomplishes two things:

1. It virtually assures computational stability of the differenced equations.

2. It permits us to analyze the energy budget of solutions to the differenced equations.

For a detailed development of the differenced equations and energy invariants the reader is referred to Lorenz's original paper.

We complete the set of model equations with a thermal equation for the ocean:

$$\frac{\partial\theta_w}{\partial t} = H_w \tag{8}$$

We solve the eqs. (1–5, 8) spectrally by ex-

panding the dependent variables in terms of spherical harmonic functions:

$$(\psi,\tau,\theta,\sigma,\chi,\theta_w) = \sum_{n=0}^{\infty}\sum_{m=-n}^{+n}(\psi_n^m,\tau_n^m,\theta_n^m,\sigma_n^m,\chi_n^m,\theta_{wn}^m)\,y_n^m(\alpha,\varphi)$$

and then truncating the series to include only certain pre-chosen harmonics. Here,

$$y_n^m(\alpha,\varphi) = \left\{\frac{2n+1}{4\pi}\frac{(n-|m|)!}{(n+|m|)!}\right\}^{1/2} P_n^{|m|}(\cos\alpha)\,e^{im\varphi}$$

where α is the colatitude, φ the longitude, and P_n^m an associated Legendre's function. Y_n^m has m oscillations running east–west around the globe and $n-|m|$ zero-crossings between the north and south poles. As is well known, the spherical harmonics comprise a complete set of orthogonal functions and satisfy the eigenvalue relation

$$\nabla^2 y_n^m = -\frac{n(n+1)}{r_e^2}y_n^m$$

where r_e is the earth's radius.

The complete set of coupled ordinary differential equations are as follows:

$$k(k+1)\frac{d\psi_k^j}{dt} = -\frac{1}{r_e^2}\sum_{\langle n,m\rangle}\sum_{\langle r,s\rangle}(\psi_n^m\psi_r^s+\tau_n^m\tau_r^s)\,r(r+1)\times E_{nrk}^{ms-j} + 2\Omega\sqrt{-1}\,j\psi_k^j - r_e^2(F_\psi)_k^j \tag{9}$$

$$k(k+1)\frac{d\tau_k^j}{dt} = -\frac{1}{r_e^2}\sum_{\langle n,m\rangle}\sum_{\langle r,s\rangle}(\tau_n^m\psi_r^s+\psi_n^m\tau_r^s)\,r(r+1)\times E_{nrk}^{ms-j} - \Omega(4\pi/3)^{1/2}\sum_{(r,s=j)}\chi_r^j \times\{2-r(r+1)-k(k+1)\}A_{1rk}^{0j-j} + 2\Omega\sqrt{-1}\,j\tau_k^j - r_e^2(F_\tau)_k^j \tag{10}$$

$$\frac{d\theta_k^j}{dt} = -\frac{1}{r_e^2}\sum_{\langle n,m\rangle}\sum_{(r,s)}(\psi_n^m\theta_s^r+\tau_n^m\sigma_r^s)\,E_{nrk}^{ms-j} + \sum_{(n,m)}\sum_{(r,s)}\frac{\sigma_n^m\chi_r^s}{2r_e^2}\{n(n+1)-r(r+1) - k(k+1)\}A_{nrk}^{ms-j} + (H_\theta)_k^j \tag{11}$$

$$\frac{d\sigma_k^j}{dt} = -\frac{1}{r_e^2}\sum_{\langle n,m\rangle}\sum_{(r,s)}(\psi_n^m\sigma_r^s+\tau_n^m\theta_r^s)\,E_{nrk}^{ms-j} + \sum_{(n,m)}\sum_{(r,s)}\frac{\theta_n^m\chi_r^s}{2r_e^2}\{n(n+1)+r(r+1) - k(k+1)\}A_{nrk}^{ms-j} + (H_\sigma)_k^j \tag{12}$$

$$-bC_p k(k+1)\theta_k^j = \sum_{\langle r,s=j\rangle}\tau_r^j\,\Omega(4\pi/3)^{1/2}\{2-r(r+1) - k(k+1)\}A_{1rk}^{0j-j} \tag{13}$$

$$\frac{d\theta_{wk}^j}{dt} = (H_w)_k^j \tag{14}$$

$\Omega = 2\pi$ day^{-1}

In the above equations the symbol $\Sigma_{\langle n,m\rangle}$ refers to that part of $\Sigma_{n=0}^{\infty}\Sigma_{m=-n}^{+n}$ that includes only the finite set of "velocity harmonics"—the harmonics chosen to represent ψ and τ. Similarly, $\Sigma_{(n,m)}$ refers to that part of $\Sigma_{m=0}^{\infty}\Sigma_{m=-n}^{+n}$ that includes only the "thermal harmonics" representing θ, σ, χ, and θ_w. To reduce the possible number of degrees of freedom, we assume that the flow is symmetric about the equator. In this case, the velocity harmonics include only functions Y_n^m for which $n-|m|$ is odd; whereas the thermal harmonics have $n-|m|$ even. The expressions A_{nrk}^{msj} and E_{nrk}^{msj} are the Adams and Elsasser integrals defined by:

$$A_{nrk}^{msj} = \int_0^{\pi}\sin\alpha\,d\alpha\int_0^{2\pi}d\varphi\,y_n^m y_r^s y_k^j$$

and

$$E_{nrk}^{msj} = \int_0^{\pi}d\alpha\int_0^{2\pi}d\varphi\left\{\frac{\partial y_n^m}{\partial\alpha}\frac{\partial y_r^s}{\partial\varphi}-\frac{\partial y_n^m}{\partial\varphi}\frac{\partial y_r^s}{\partial\alpha}\right\}y_k^j.$$

James (1973) gives a formula for evaluating these integrals. In eq. (13), it can be shown that $A_{1rk}^{0J-J}=0$ unless $r=k\pm1$. Thus θ_n^m is coupled to τ_{n+1}^m and τ_{n-1}^m via the thermal wind relation.

Under adiabatic conditions, the spectrally-truncated differenced equations conserve the sum of the spectral truncations of (6) and (7). We shall refer to

$$K_n^m = \frac{\Delta p}{4\pi g r_e^2}\{|\psi_n^m|^2+|\tau_n^m|^2\}\,n(n+1)\,(2-\delta_{0m}),\qquad m\geq 0$$

and

$$A_n^m = \frac{2bC_p\Delta p}{g(4\pi)^{1/2}} \frac{\{|\theta_n^m|^2 + |\sigma_n^m|^2\}(2-\delta_{0m})}{\sigma_0^0 + \{\sum_{(r,s)} (|\theta_r^s|^2 + |\sigma_r^s|^2) - \theta_0^{02}\}^{1/2}},$$

$$n \neq 0,\ m \geq 0$$

as the kinetic and available potential energy in mode n–m.

We solve the prognostic equations (9–12, 14) with a predictor/corrector time-stepping scheme. Although there is no prognostic equation for χ, we can obtain a set of diagnostic equations for χ_n^m in terms of the prognostic variables ψ, τ, θ, σ, θ_w by replacing (13) with its time derivative and substituting from eqs. (10) and (11) for $d\tau_r^s/dt$ and $d\theta_k^s/dt$. The resulting equations can be simplified in their general form and solved by Gaussian elimination on the computer.

It remains to specify the friction and heating terms. They are:

$$F_\psi = -\frac{k^*}{2}\overset{(a)}{\nabla^2\psi_s} - \overset{(e)}{E_\psi} \tag{15}$$

$$F_\tau = +\frac{k^*}{2}\overset{(a)}{\nabla^2\psi_s} - 2l\overset{(b)}{\nabla^2\tau} - \overset{(e)}{E_\tau} \tag{16}$$

$$H_\theta = -\overset{(c)}{k_T(\theta-\theta^*)} + \frac{\lambda_1}{2}\overset{(d)}{(\theta_w-\theta_s)} - \overset{(e)}{E_\theta} \tag{17}$$

$$H_\sigma = -\overset{(c)}{h(\sigma-\sigma^*)} - \frac{\lambda_1}{2}\overset{(d)}{(\theta_w-\theta_s)} - \overset{(e)}{E_\sigma} \tag{18}$$

$$H_w = -\overset{(d)}{\lambda_2(\theta_w-\theta_s)} \tag{19}$$

where ψ_s and θ_s are the surface stream function and air temperature (eq. 23). The terms designated by letters represent the effects of:

(a) friction with the ground, and

(b) between levels;

(c) net radiational convergence, mean sensible and latent heat transfer and small-scale vertical mixing in driving the atmosphere toward a steady state: $\theta = \theta^*$, $\sigma = \sigma^*$ that would prevail in the absence of large-scale flow;

(d) anomalous latent and sensible heat exchange between the ocean and lower troposphere; and

(e) small-scale horizontal mixing.

The terms (a) can, if one desires, be thought of as an Ekman friction in which case

$$w_{\text{Ekman}} = \frac{\Delta p k^*}{\varrho_s g}\left(\frac{\nabla^2\psi_s}{f}\right) \tag{20}$$

In (d) the anomalous heat flux from ocean to atmosphere is assumed to obey:

$$\text{flux} = \lambda(\theta_w - \theta_s) \tag{21}$$

so that

$$\lambda_1 = \frac{(\frac{4}{3})^\kappa g\lambda}{\Delta pCp} \quad \text{and} \quad \lambda_2 = \frac{\lambda}{\varrho_w C_{pw} D} \tag{22}$$

where D is the depth of the oceanic mixed layer (assumed constant) and suscript w refers to ocean variables. We express the surface variables in terms of the model variables by:

$$\psi_s = \psi - \gamma\tau,\ \theta_s = \theta - \gamma\sigma \tag{23}$$

If ψ and θ are linear in pressure then $\gamma = 2$. However, it is more realistic to assume that the variables are linear in height, in which case $\gamma = 1.6$ for a "standard atmosphere".

The above extremely crude parameterization abstracts the atmospheric heating field into two parts: a part that is correlated with the temperature of the lower bounding surface and a part that is independent of it. Both parts are characterized by equilibrium states (θ^*, σ^*; θ_w) and return time scales ($1/k_T$, $1/h$; $2/\lambda_1$). we have tentatively assumed that these time scales are equal:

$$\frac{1}{k_T} = \frac{1}{h} = \frac{2}{\lambda_1}$$

and adjusted their values, along with the other parameters in (15–19), to obtain a model general circulation whose spectral energetics agree reasonably well with Saltzman's (1970) summary of the observational data. The values we arrived at are the following:

$$\frac{1}{k^*} = 2.55 \text{ days}; \quad \frac{1}{l} = 67.9 \text{ days}$$

$$\frac{1}{k_T} = \frac{2}{\lambda_1} = \frac{1}{h} = 10.2 \text{ days}$$

$$\frac{1}{\lambda_2} = 41.6 \text{ days and } \infty \text{ days}$$

$$\sigma^* = 12.5 \text{ C}$$

Table 1. *The set of harmonics used in the experiments described in this paper*

Harmonic n–m refers to y_n^m

Velocity harmonics				
5–0	8–3	11–6	14–9	17–12
3–0	6–3	9–6	12–9	15–12
1–0	4–3	7–6	10–9	13–12
Thermal harmonics				
6–0				
4–0	7–3	10–6	13–9	16–12
2–0	5–3	8–6	11–9	14–12
0–0	3–3	6–6	9–9	12–12

and

$$\begin{Bmatrix} E_\psi \\ E_\tau \\ E_\theta \\ E_\sigma \end{Bmatrix} = \begin{Bmatrix} \sum\limits_{\langle n,\, m\rangle} -\dfrac{n^2(n+1)^2}{r_e^2} \\ \sum\limits_{(n,\, m)} n(n+1) \end{Bmatrix} (0.00016\,\mathrm{day}^{-1}) \begin{Bmatrix} \psi_n^m \\ \tau_n^m \\ \theta_n^m \\ \sigma_n^m \end{Bmatrix} y_n^m$$

The value of k^* corresponds to $\Delta p k^*/\varrho_s g = 3.12$ cm sec^{-1} in (20). Our choice of λ_1 corresponds to $\lambda = 22.3$ ly day^{-1} deg^{-1} which is smaller than the value of 63.1 used by Doos (1962). The two extreme values of λ_1 correspond to $D = 9.3$ m and $D = \infty$ (constant temperature ocean). The eddy viscosity is quite modest; at the highest wavenumbers considered it amounts to only about one fourth the ground friction. θ^*, which is assumed proportional to y_2^0 is sketched in Fig. 4.

We do not permit the model to determine its own globally-averaged temperature but set $\theta_0^0 = \theta_{w0}^0 = 0$ throughout. Thus the only globally-averaged temperature of physical significance is σ_0^0, which is porportional to the average temperature difference between 250 mb and 750 mb. For σ_0^0 only, we use

$$(H_\sigma)_0^0 = -\left(h + \frac{\lambda_1}{2}\right)(\sigma_0^0 - \sigma_0^{*0}) \tag{24}$$

instead of (18). σ^* is chosen so that the equilibrium σ is less than its value in Nature. In this way, we model implicitly the destabilizing influence of water vapor in the earth's atmosphere.

The computer program that solves the model equations is written in a general form that accepts any basic set of spherical harmonic functions. The choice of specific set is to some extent arbitrary, but the chosen harmonics should accommodate spectral energy transfers analogous to those which are known to be important in the real atmosphere. Table 1 presents the set of harmonics we have used in the experiments in section 3. It consists of a zonal flow and 4 zonal wavenumbers, each with 3 degrees of freedom in the north–south direction. The chosen zonal harmonics are just sufficient to resolve the classical three-cell (two Hadley, one Ferrel) structure of the general circulation.

Our restrictive choice of harmonics drastically under-represents the influence of the higher wavenumbers in the flow, whose principal dynamical effect is assumed to be the destruction of accuracy in deterministic forecasts on a time scale of T_A.[1] We assume a priori that for times longer than T_A, only the *statistics* of the large-scale flow are pertinent; and we direct our research to the questions:

1. How do the stationary statistics of our atmosphere change when the properties of the ocean model are changed?

2. How long must one average to detect these statistical changes above the random noise in the large-scale flow?

Our approach is strictly valid only if unresolved small scales exert no ocean-sensitive effects on the large-scale *statistics*, and if the random noise in large-scales can be reasonably well mimicked by a model that includes *only* large scales.

While a rigorous justification of our method awaits careful experimentation with higher-resolution models, we are encouraged by the resemblence of some statistics of our simple model with those based on real observations. Fig. 1 compares the model energy cycle, averaged over 357 days, with Saltzman's (1970) observed energy cycle (band averaged in zonal wavenumber m) for winter and summer. The overall agreement between model and atmosphere is good except for the model wavenumber 3. Further experiments have shown that the situation improves considerably when we include mountain ranges and large-scale stationary heating, which are known to force the very long waves. Fig. 2 compares the model average flow fields with the observations. Generally speaking, our simulation resembles the

[1] The time required for the propagation of order one error from the smallest scales resolved in our model to the largest scales was found to be less than three days.

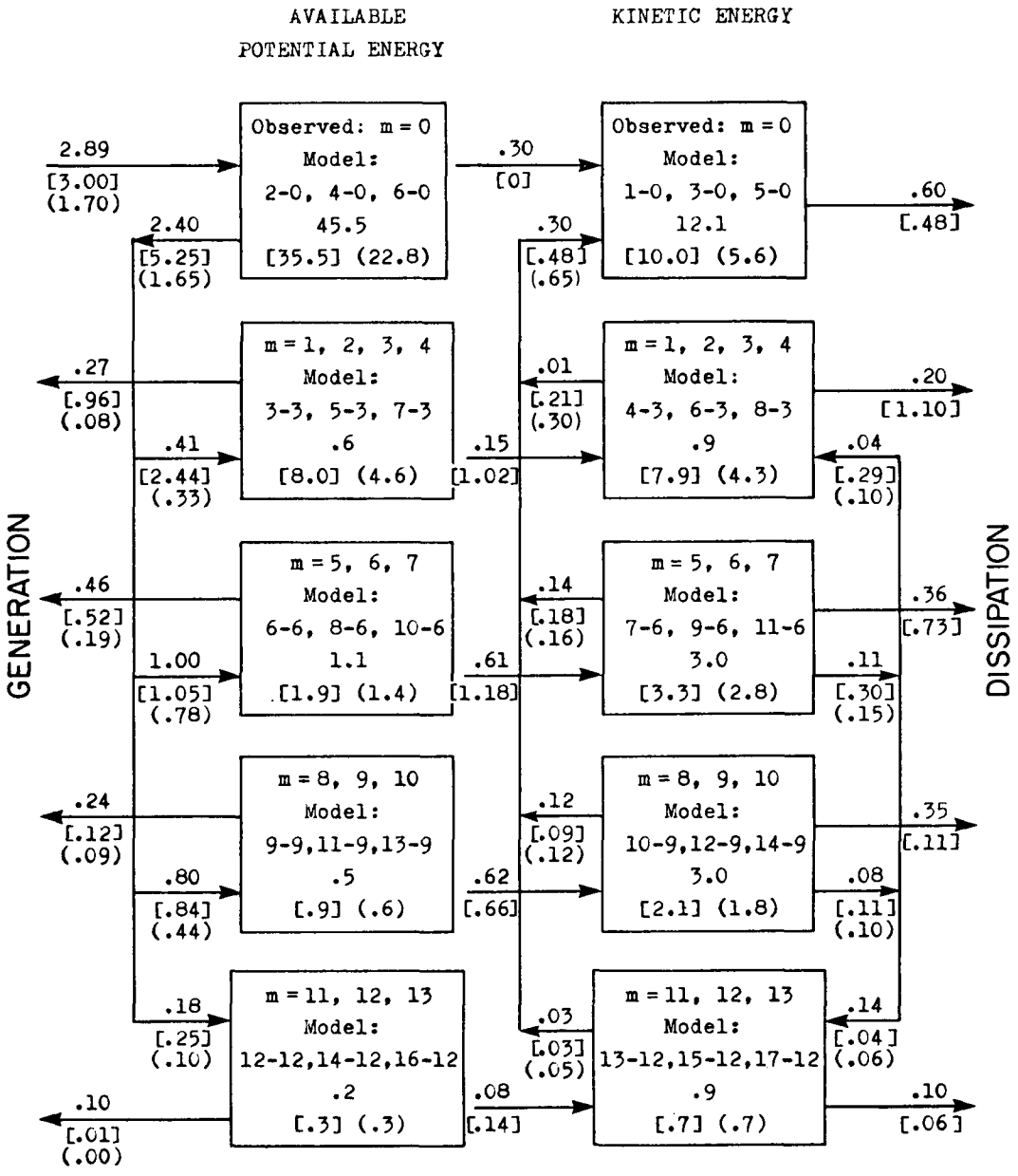

Fig. 1. Comparison of the model energy cycle averaged over one year with Saltzman's (1970) observations (band averaged in zonal wavenumber m) for winter (in brackets) and for summer (in parentheses). Boxes give energy in 10^5 joule m^{-2} and the arrows give energy flux in watt m^{-2}. The definition of energy quantities and the spectral truncation differ between our model and the Saltzman data, so that the comparison is not intended to be exact. The conversion arrows give the gain of kinetic energy in each band from the total available potential energy.

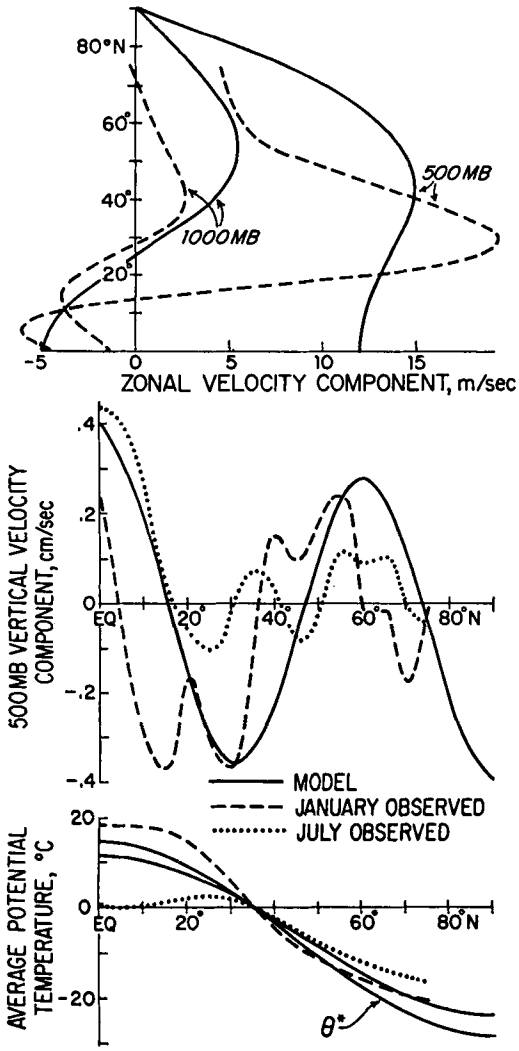

Fig. 2. Average flow quantities in the model and in the real atmosphere. The average temperature presented is the actual temperature minus the temperature at 35 N. Observations are from Oort & Rasmusson tables A 8, A 9, and F 8.

atmosphere under winter conditions except for the imposed equatorial symmetry.

The method of spectral solution has been applied extensively to Lorenz's model (minus the ocean) by other investigators. However, ours is the first application (of which we are aware) that allows the static stability σ to vary in space. The static stability is known from both theory and experiment to exert an important control on flow in rotating, differentially-

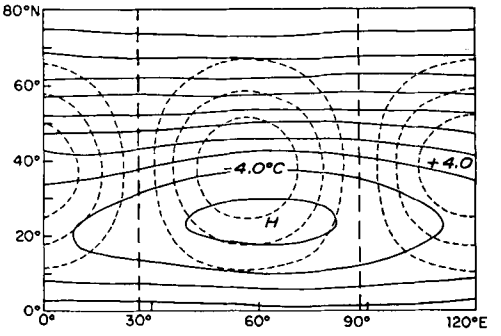

Fig. 3. SST anomaly pattern (broken line) and average surface stream function in WM. The SST extrema are ± 4.0 C. The maximum wind speed is 6 m sec^{-1}.

heated fluids. Moreover, static stability and SST may be correlated in Nature; Namias (1973) has shown that when SST anomalies are large, there is sometimes good correlation between SST anomaly and the thickness (temperature) of the air below 750 mb.

Solving eqs. (9–14) with the harmonics in Table 1 amounts to time-stepping 164 coupled nonlinear real ordinary differential equations. With a time step of 0.25 days, one year's climatic simulation requires about 3.25 minutes of CPU time on a 7600 computer at a cost of about $32.

3. Three experiments

In this section we present the results of three experiments in which the model equations were solved with the harmonics in Table 1 subject to the forcing (15–19, 24). The three experiments are:

I. A control run (CR) in which the sea surface temperature is fixed ($\lambda_2 = 0$) and depends only on the latitude.

II. A run (WM) with fixed large-amplitude SST anomalies that resemble the observed anomalies in shape.

III. A mixed-layer run (ML) in which the ocean is free ($\lambda_2 \neq 0$) to adjust its temperature by heat exchange with the atmosphere. The mixed layer depth was taken to be 10 m.

The mixed layer experiment was actually performed first. We then used the time average of the zonally averaged sea temperature in

Table 2. *Energy cycles of the three experiments*

Quantity	m	357-day average I–CR	357-day average II–WM	357-day average III–ML	Estimated $\hat{\sigma}$ I	Estimated $\hat{\sigma}$ II	Estimated $\hat{\sigma}$ III	Significance parameter $S_{I,II}$	Significance parameter $S_{I,III}$
Kinetic energy	0	12.06	11.90	12.32	0.10	0.12	0.24	0.76	0.77
in zonal	3	0.94	1.00	0.87	0.09	0.07	0.11	0.43	0.33
wave number m	6	3.02	2.80	2.82	0.20	0.14	0.36	0.63	0.35
(10^5 joule m^{-2})	9	2.95	3.00	2.80	0.31	0.23	0.26	0.10	0.26
	12	0.92	0.87	0.82	0.07	0.06	0.40	0.40	0.95
Available pot.	0	45.46	45.57	45.73	0.38	0.55	0.75	0.11	0.23
energy in m	3	0.64	0.74	0.62	0.04	0.04	0.06	1.19	0.12
(10^5 joule m^{-2})	6	1.07	1.02	1.15	0.08	0.07	0.12	0.35	0.38
	9	0.51	0.54	0.50	0.05	0.05	0.05	0.28	0.19
	12	0.17	0.16	0.17	0.01	0.01	0.01	0.75	0.02
Conversion	0	0.30	0.29	0.33	0.02	0.01	0.02	0.43	0.63
of APE to	3	0.15	0.19	0.15	0.02	0.02	0.02	1.00	0.07
KE in m	6	0.61	0.54	0.56	0.06	0.04	0.05	0.70	0.51
(watt m^{-2})	9	0.62	0.68	0.60	0.07	0.07	0.06	0.38	0.16
	12	0.08	0.07	0.08	0.02	0.02	0.02	0.29	0.12
Generation of	0	2.89	2.87	2.85	0.05	0.08	0.10	0.14	0.21
APE in m	3	−0.27	−0.27	−0.26	0.02	0.02	0.03	0.07	0.21
(watt m^{-2})	6	−0.46	−0.44	−0.50	0.04	0.03	0.06	0.35	0.38
	9	−0.24	−0.25	−0.23	0.02	0.02	0.02	0.27	0.21
	12	−0.10	−0.09	−0.09	0.01	0.005	0.01	0.74	0.45
Transfer of	0	−2.39	−2.39	−2.34	0.05	0.07	0.08	0.04	0.35
APE to	3	0.41	0.45	0.39	0.03	0.04	0.04	0.64	0.20
m by	6	1.00	0.92	1.00	0.08	0.07	0.09	0.54	0.03
temperature	9	0.80	0.86	0.77	0.08	0.08	0.08	0.38	0.18
advection	12	0.18	0.16	0.18	0.03	0.02	0.02	0.12	0.01
(watt m^{-2})									
Nonlinear	3	0.01	0.02	0.01	0.01	0.01	0.004	0.75	0.08
transfer of	6	0.14	0.13	0.10	0.01	0.01	0.01	0.54	1.27
KE to zonal	9	0.12	0.12	0.12	0.01	0.01	0.02	0.04	0.05
flow by m	12	0.03	0.03	0.02	0.003	0.003	0.004	0.33	1.53
(watt m^{-2})									
Gain of KE by	3	0.04	0.03	0.04	0.02	0.02	0.01	0.28	0.10
m due to wave	6	−0.11	−0.08	−0.07	0.03	0.02	0.02	0.48	0.68
interactions	9	−0.08	−0.10	−0.08	0.03	0.03	0.02	0.28	0.01
(watt m^{-2})	12	0.14	0.14	0.11	0.01	0.02	0.01	0.03	1.20
Gross static stability (10^5 joule m^{-2})		166.01	165.98	165.78	0.19	0.17	0.23	0.10	0.55

ML for the fixed ocean in CR. For experiment II we superimposed the longitudinally-sinusoidal SST anomaly pattern of Fig. 3 on the standard ocean of CR. Because the anomalous heating field in experiment II resembles the heating fields hypothesized in various linear theories of atmospheric response to large-scale stationary heating (for example, Smagorinsky, 1953), we will refer to experiment II as the "weak monsoon" (WM) experiment. Each of the three experiments was allowed several months of simulated time in which to reach statistical equilibrium. Then the equations were stepped for 357 days and all the data was saved. Some averaged properties of CR have already been given in section 2.

We begin our analysis of the three experiments by showing that the different ocean models cause no statistically significant difference in the globally-averaged energy cycle. First, however, we describe the very simple format we have used to compare statistical

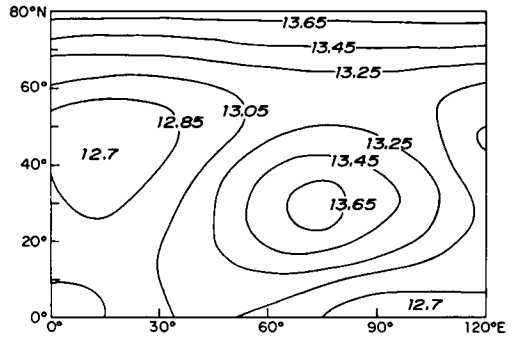

Fig. 4. Average static stability, σ, in experiment WM (degrees centigrade).

averages: Let $V(t)$ be any quantity and suppose we wish to compare the average of V in run 1 with its average in run 2. We divide each run of length T into N subintervals of equal length T/N and form the average of V over each subinterval. Let $\overset{i}{V}$ be the average over the ith subinterval. Then the average of V over the entire record in run j is:

$$\bar{V}_j = \frac{1}{N}\sum_{i=1}^{N} \overset{i}{V}_j$$

We assume that the subintervals are sufficiently long so that $\overset{i}{V}$ and $\overset{k}{V}$ are independent random variables if $i \neq k$. Then the variance of $\overset{i}{V}$, assumed independent of i, is given by the (unbiased) estimator:

$$\sigma^2 = \frac{1}{N-1}\sum_{i=1}^{N} (\overset{i}{V} - \bar{V})^2$$

and the standard deviation of $\bar{V}$ is:

$$\hat{\sigma} = \sigma/N^{\frac{1}{2}}$$

We define a "significance parameter" for the difference between $\bar{V}_1$ and $\bar{V}_2$ by:

$$S_{1,2} = |\bar{V}_1 - \bar{V}_2|/(\hat{\sigma}_1 + \hat{\sigma}_2) \qquad (25)$$

When $S_{1,2}$ is larger than unity then $\bar{V}_1$ and $\bar{V}_2$ differ by a statistically significant amount.[1]

[1] For example, if V_1 and V_2 are Gaussian with $\langle V_1 \rangle = \langle V_2 \rangle$, then the probability that $S_{1,2}$ exceeds unity is 31.7%. Most of the quantities analyzed appear not to be Gaussian, however.

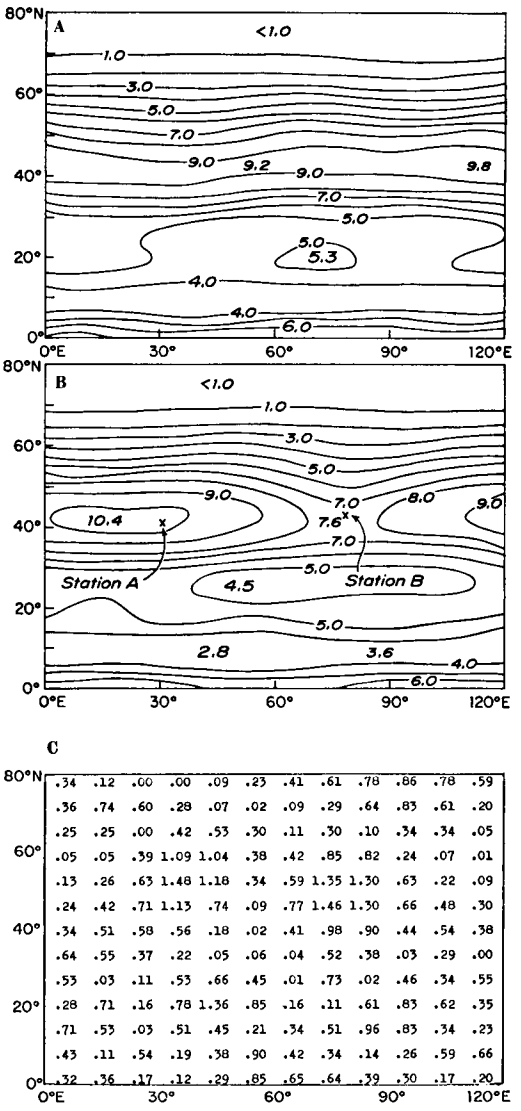

Fig. 5. (*a*) The variance of sea-level potential temperature $(\overline{\theta_s'})^2 = \overline{\theta_s^2} - \bar{\theta}_s^2$ in deg^2 in CR and (*b*) in WM; and (*c*) the field of significance parameter for the averages in (*a*) and (*b*).

For large $S_{1,2}$ we have the following (biased) estimate of the quantity T_s defined in section 1:

$$T_s \sim \frac{1}{S_{1,2}^2} T \qquad (26)$$

For $S_{1,2} < 1$ we can say only that $T_s > T$. If $V(t)$ contains significant energy at periods

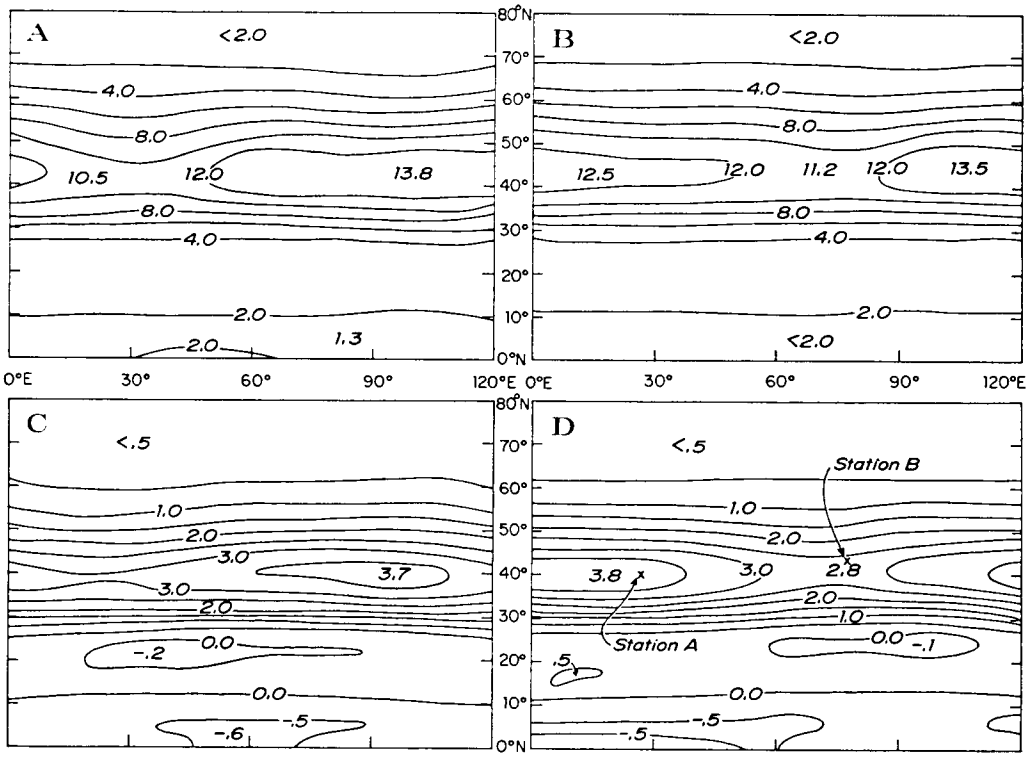

Fig. 6. (*a*) The variance of potential temperature at 500 mb $\overline{(\theta')^2}$ in CR and (*b*) in WM; and (*c*) the transient conversion $\overline{w'\theta'}$ (deg cm sec^{-1}) in CR and (*d*) in WM.

longer than T/N then the above method underestimates the significance of the difference between $\bar{V}_1$ and $\bar{V}_2$. Since all of the model variables analyzed in the above manner had computed spectra that were white or blue at periods exceeding one month, we have chosen T = 357 days and $N = 10$.

Table 2 summarizes the global energy cycles of the three experiments. The quantities tabulated are the same as those diagramed in Fig. 1 for CR only. From the last two columns of Table 2 we see that if statistical differences exist between the three energy cycles, they apparently cannot be detected above the random noise in time averages of one year or less.

Of course, it is not especially surprising that space–time averages should be similar in the three experiments, because all three have the same time–longitude averaged sea temperature. It is more likely that the experiments have different average spatial distributions of certain quantities and that the distributions are correlated in some way with the SST anomaly pattern. Fig. 3 shows the average surface stream function in WM. A stationary signal is present in the form of a low level ridge centered near the meridian of maximum cooling. At upper levels, the ridge becomes a trough that is barely detectable in the strong westerly flow. The signal in Fig. 3 is statistically significant ($S_{I,II}$ exceeds 3.0) and agrees approximately with linear theory. It is interesting, however, that the maximum response occurs in the subtropics (25 N lat.) and not at the latitude of maximum anomalous heating (44 N). This is apparently because the strong nonlinearities associated with mid-latitude storms would completely disrupt a weak stationary wave. The average stream function in CR is independent of longitude.

The large SST anomalies in WM have no direct influence on the average flow at middle and high latitudes; but they may affect the travelling storms that pass through these re-

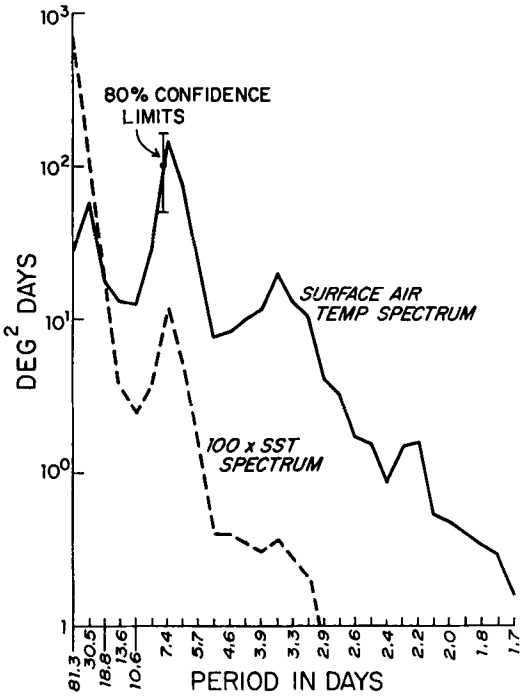

Fig. 7. Spectra of surface air temperature and 10 × sea surface temperature at 45 N in ML. Spectra are band-averaged over 5 frequencies.

gions. Fig. 4 shows the average static stability field in WM. A region of low static stability occurs just downwind of the region of maximum surface heating and a stable region occurs downwind of the maximum cooling. From linear baroclinic instability theory, we anticipate that the storms might intensify as they pass through the region of low static stability and weaken in the region of high stability. One possible index of storm intensity is the variance of potential temperature which is mapped at sea level in Fig. 5*a* for CR and Fig. 5*b* for WM. The field of $S_{I,II}$ for the averages in Figs. 5*a–b* is given in Fig. 5*c*. From Fig. 5*b* it does indeed appear that storms intensify in the region of low static stability. A spectral analysis of the temperature records at stations *A* and *B* in Fig. 5*b* verifies that the larger variance of θ_s at station *A* is primarily caused by the intensification of disturbances with periods between 3 and 9 days.

Figs. 6*a–b* show the variance of potential temperature at 500 mb in the same two experiments. Again in WM, $\overline{(\theta')^2}$ is a maximum in the region of low static stability. Somewhat surprisingly, however, $\overline{(\theta')^2}$ also shows a maximum in CR (Fig. 6*a*). The maximum in CR is not correlated with a minimum in static stability and occurs purely by chance.

Still another index of storm intensity is the quantity

$$\overline{w'\theta'} = \overline{w\theta} - \overline{w}\,\overline{\theta} \tag{27}$$

where w is the vertical velocity (cm sec^{-1}) at 500 mb. The above expression is proportional to the conversion of potential to kinetic energy by transient motions. The field of (27) is contoured in Fig. 6*c* for CR and in Fig. 6*d* for WM. In Fig. 6*d* the intensity index is 40% greater at station *A* than at station *B*. However, as we see from Fig. 6*c*, the model atmosphere is so noisy that a disparity of more than 20% can be accounted for by chance alone. In summary, it appears that SST anomalies as big as ±4C can influence the pattern of storm intensity if they persist for as long as a year. However, the effect they produce is no more than twice as large as could be expected by chance alone.

Experiment ML developed SST anomalies of about the same magnitude and extent as those observed in Nature. As in the observations (Namias, 1972), the model SST anomalies show good correlation with the atmospheric flow on the scale of quasi-stationary waves (model wavenumber $m = 3$). In the model, at least, this correlation is not surprising; because $\lambda_2 < \lambda_1$ the model ocean acts like a low-pass filter to the atmosphere with a cutoff at period 260 days for $D = 10$ m. Fig. 7 shows the surface air temperature and SST spectra at 45 N in ML. The peaks at 30 days, 7 days, and 3.5 days correspond to waves with discrete wavenumbers $m = 3$, 6, 9. In the model, as in the real atmosphere, most of the energy is at periods between 1 and 30 days; but the SST spectrum is red. Table III gives the contribution of the various zonal wavenumbers to the globally-averaged temperature variances in the air and water and to the total correlation coefficient, r, between the air and SST anomalies. Although most of the air temperature variability occurs in the storm scales ($m = 6$, 9), the ocean, with its high impedance to short time scales, responds chiefly to $m = 0$ and 3 which together account for 94%

of the total correlation between air and SST anomalies. We have spectrally analyzed the globally-averaged surface air temperature variance and found that periods longer than 20 days account for 75% and 65% respectively of the variance in wavenumbers 0 and 3.

We have visually analyzed the fields of SST and 24-day-running-mean-averaged stream function at 750 mb for the full record in ML. We find that the SST anomaly pattern changes most rapidly during blocking episodes when the kinetic energy in wavenumber 3 is a maximum. Such episodes occur at irregularly spaced intervals of 50 to 75 days. Between the episodes the SST pattern shows a remarkable persistence.

In order to determine whether or not the SST anomaly patterns affect the weather in ML we have tried the following procedure: We have computed θ_w from eqs. (14, 19) using the surface air temperature θ_s obtained in CR. We refer to the $\theta_w(t)$ so obtained as the "slave ocean" for run CR. In both the slave ocean and the ocean in ML the maximum SST anomalies occur near 50 N. Fig. 8 shows the longitude, $\varphi_0(t)$, of the maximum (positive) SST anomaly at 50 N for ML and for the slave ocean in CR. In both cases the glob of warm water moves to the east on average.

We now introduce an averaging method which has proved useful in analyzing the slowly moving SST fields. At every time step we determine $\varphi_0(t)$ and translate the picture of the flow until $\varphi_0(t)$ coincides with the zero meridian. The average of all the translated pictures—which we call the "composite average"—is the average flow seen by an observer moving with the SST anomaly. We emphasize, however, that all of the quantities so averaged are themselves measured in the reference frame attached to the earth.

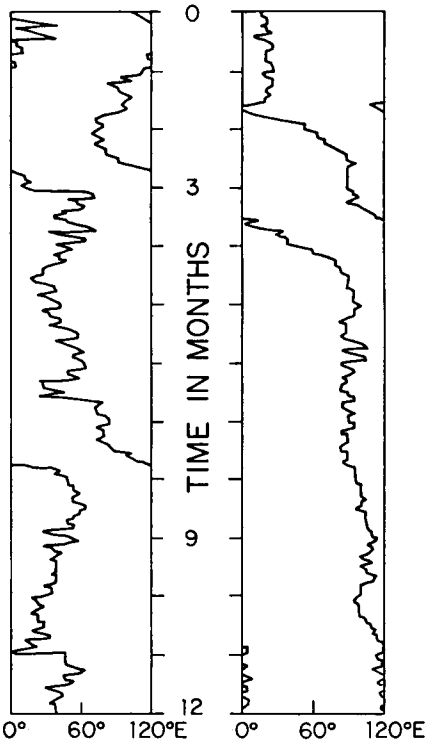

Fig. 8. The longitude, $\varphi_0(t)$, of the maximum positive SST anomaly at 50 N for the slave ocean in CR (left) and for ML (right).

Table 3. *The contribution of the various zonal wavenumbers m to the globally-averaged variances of* $\theta_s' \equiv \theta_s - \bar{\theta}_s$ *and* $\theta_w' \equiv \theta_w - \bar{\theta}_w$ *and their average spatial correlation coefficient r*

The bar (⁻) denotes time average; the brackets ([ ]) denote space average; and $r \equiv [\theta_s^1 \theta_w^1]/([(\theta_s^1)^2]^{1/2}[(\theta_w^1)^2]^{1/2})$

Zonal wavenumber (m)	$\overline{[(\theta_s')^2]}$	$\overline{[(\theta_w')^2]}$	$\overline{[\theta_w'\theta_s']}$	$\bar{r}$
0	0.23	0.033	0.032	0.045
3	1.30	0.065	0.072	0.095
6	2.17	0.006	0.007	0.009
9	1.11	0.0004	0.0004	0.0006
12	0.57	0.0001	0.0002	0.0003
Total	5.38	0.105	0.111	0.149

Fig. 9*a* shows the composite average SST anomaly pattern in ML and the corresponding composite average of the 24-day-running-mean-averaged stream function anomaly at 750 mb. As in the real observations (Namias, 1972), warm spots are correlated with anomalous geostrophic wind from the south and high pressure to the east. Fig. 9*b* shows the corresponding composite averages for the slave ocean in CR. In Fig. 9*b* the SST amplitude and the phase lag between pressure and temperature are smaller than in Fig. 9*a*; but these differences can be quantitatively explained by taking into account the fact that the slave ocean adjusts its

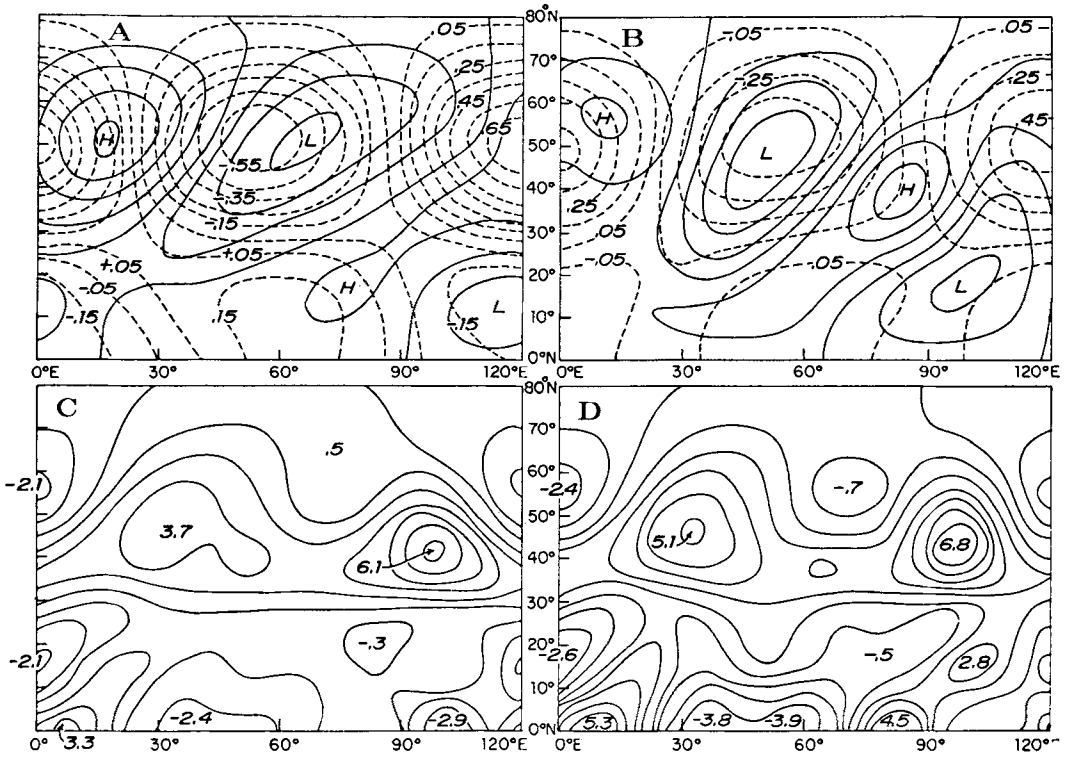

Fig. 9. (*a*) The composite average SST anomaly (broken line) and 24-day-running-mean-averaged stream function anomaly at 750 mb for ML and (*b*) for the slave ocean in CR. The maximum anomalous wind speed is 1.6 m sec^{-1}. (*c*) The composite average transient conversion (deg cm sec^{-1}) in ML and (*d*) in CR.

temperature without changing the temperature of the overlying air. Except for the slight difference in phase lag, the composite averaged atmospheric flow fields (such as the 750 mb pressure in Figs. 9*a–b*) are remarkably similar in ML and CR. This similarity supports the view that SST anomaly patterns are the result rather than the cause of low-frequency motions in the atmosphere.

Do the SST anomalies affect the pattern of storm intensity in ML? The composite average static stability in ML and CR show similar patterns, although there is a slight (0.1 C) tendency for lower stability over warm water in ML. Figs. 9*c–d* show the composite average conversion of potential to kinetic energy by transients in ML and in CR. The quantity contoured is:

$$\overline{w\theta - \overline{w}^{f}\overline{\theta}^{f}}^{m}$$

where (^{f}) denotes the time average in the reference frame fixed on the earth and (^{m}) denotes the moving (composite) time average. The storms are actually less intense over warm water in ML than in the corresponding location in CR. The differences between Figs. 9*c–d* are therefore almost certainly not statistically significant.

4. Conclusion

The experiments summarized in section 3 *suggest* that the atmosphere may simply be too noisy to be much affected by mid-latitude SST anomalies on time scales over which the anomalies are themselves predictable. However, this conclusion may depend critically on the many simplifying assumptions we have made, especially our rather extreme abstraction of the atmospheric heating field in which we explicitly neglect complicated radiation and condensation processes. Even accepting the format

of eqs. (15–19), arguments can no doubt be made that the values of the forcing coefficients should be greater or smaller than the values we have used. Here, we simply restate that our values for the atmospheric friction and heating coefficients were arrived at by the somewhat novel approach of tuning the model to the observed energy cycle. This method may be preferable to a direct estimation of the forcing parameters, because it incorporates the difficulty of allowing for the effect of the infinite vertical diffusion rate within layers upon the average fluxes of momentum and heat. To oceanographers the ten-meter mixed layer will seem to shallow; but we can easily argue that λ should be two or three times the value quoted in section 2, in which case D could be as large as 30 m with no change in λ_2. More serious, perhaps, is our neglect of ocean currents. In mid-latitudes, at least, anomalous north–south advection of the mean horizontal temperature gradient in the ocean could conceivably compete with anomalous surface heating as the cause of SST anomalies. Finally, by omitting continents, we have neglected important sources of warm and cold air.

However, granting all of the above objections, the results of this study may still be noteworthy both because of the great current interest in air/sea interactions and because the large primitive equation models (which do the best job of simulating climate) cannot yet be run economically enough to answer statistical questions about what is essentially a statistical problem.

Acknowledgements

This work was supported by the Office of Naval Research under Grant N00014-69-A-0200-6043. We wish to thank Jerome Namias for many interesting conversations.

REFERENCES

Doos, B. R. 1962. The influence of exchange of sensible heat with the earth's surface on the planetary flow. *Tellus 14*, 133–147.

James, R. W. 1973. The Adams and Elsasser dynamo integrals. *Proc. R. Soc. Lond. A 331*, 469–478.

Lorenz, E. N. 1960. Energy and numerical weather prediction. *Tellus 12*, 364–373.

Namias, J. 1959. Recent seasonal interactions between North Pacific waters and the overlying atmospheric circulation. *J. Geophys. Res. 64*, 631–646.

Namias, J. 1972. Space scales of sea-surface temperature patterns and their causes. *Fishery Bull. 70*, 611–617.

Namias, J. 1973. Thermal communication between the sea surface and lower troposphere. *J. Phys. Oceanogr. 3*, 373–378.

Oort, A. H. & Rasmusson, E. M. 1971. *Atmospheric circulation statistics*. NOAA professional paper 5.

Saltzman, B. 1970. Large scale atmospheric energetics in the wavenumber domain. *Rev. Geophys. Space Phys. 8*, 289–302.

Smagorinsky, J. 1953. The dynamical influence of large-scale heat sources and sinks on the quasi-stationary mean motions of the atmosphere. *Quart. J. R. Met. Soc. 79*, 342–366.

КРУПНОМАСШТАБНЫЕ ВЗАИМОДЕЙСТВИЯ ОКЕАНА И АТМОСФЕРЫ, ОСНОВАННЫЕ НА ПРОСТОЙ МОДЕЛИ ОБЩЕЙ ЦИРКУЛЯЦИИ

Двухуровенная атмосферная модель Лоренца (1960) комбинируется с моделью океана в виде «медной плиты» с целью получения простой модели для изучения влияния крупномасштабных аномалий температуры поверхности океана (ТПО) на динамику атмосферы. При наличии 164 степеней свободы атмосферная модель весьма детально имитирует наблюдаемый в северном полушарии энергетический цикл. В трех экспериментах, каждый продолжительностью в год, рассматривается океан: (*a*) с фиксированной температурой, которая зависит только от широты, (*b*) с фиксированными аномалиями ТПО и (*c*) с температурой, определяемой тепловым обменом с воздухом. Только в случае (*b*) наблюдаются существенные динамические эффекты. Последние состоят из слабой муссонной реакции в субтропиках и тенденции вихрей интенсифицироваться над областями теплой воды в более высоких широтах. В эксперименте (*c*) развиваются аномалии ТПО, напоминающие наблюдаемые аномалии; однако атмосфера и океан в (*c*) незначительно отличаются от атмосферы и пересчитанного «рабского океана» в (*a*), даже если течения осреднены в системе координат, движущейся вместе с аномалиями. Результаты наводят на мысль, что атмосфера обладает слишком большими шумами, чтобы воспринимать влияние аномалий ТПО в масштабе времени, в течение которого аномалии сами могут быть предсказаны.